Research Article **Open Access**

Xing-Yuan Wang, Yi-Lun Wang, Suo Wang, Bo Li, Xiao-Wei Zhang, Lun Dai*, and Ren-Min Ma*

Lasing Enhanced Surface Plasmon Resonance Sensing

DOI 10.1515/nanoph-2016-0006
Received September 4, 2015; accepted December 21, 2015

Abstract: The resonance phenomena of surface plasmons has enabled development of a novel class of non-contact, real-time and label-free optical sensors, which have emerged as a prominent tool in biochemical sensing and detection. However, various forms of surface plasmon resonances occur with natively strong non-radiative Drude damping that weakens the resonance and limits the sensing performance fundamentally. Here we experimentally demonstrate the first lasing-enhanced surface plasmon resonance (LESPR) refractive index sensor. The figure of merit (FOM) of intensity sensing is ~84,000, which is about 400 times higher than state-of-the-art surface plasmon resonance (SPR) sensor. We found that the high FOM originates from three unique features of LESPR sensors: high-quality factor, nearly zero background emission and the Gaussian-shaped lasing spectra. The LESPR sensors may form the basis for a novel class of plasmonic sensors with unprecedented performance for a broad range of applications.

Keywords: Surface plasmon resonances, stimulated emission, plasmon lasers, sensors

Surface plasmons are quasiparticles of coupled photons and electrons excited at the metal surface [1]. They can be tightly localised at the metal surface and thus highly sensitive to its dielectric environment. Surface plasmon sensors operate on the principle that small changes in refractive index at the vicinity of metal surface can result in a shift of surface plasmon resonance, which can be detected at optical far field, allowing non-contact, real-time and label-free sensing and detection [2–6]. In the past two decades, the surface plasmon resonance (SPR) sensors based on propagating surface plasmon polaritons have become a prominent tool for characterising and quantifying biomolecular interactions and are perhaps the most extensively utilised optical biosensors [3, 7, 8]. However, the propagating surface plasmons on flat surface cannot be directly excited due to their large momentum. In most SPR sensors, the Kretschmann configuration of attenuated total reflection is used to excite surface plasmons, which requires precise adjustment of the incident angle of the probing radiation [3, 7, 8]. Therefore, it remains a challenge for SPR sensors to have point-of-care performance and satisfy modern nanobiotechnology architectures [3, 7, 9].

Localised surface plasmons (LSPs) are another type of surface plasmons that have begun to be used in sensors recently [4–6]. In contrast to its propagating counterpart, LSPs can be excited directly in metallic structures with dimensions less than half the wavelength. Single metal particle with tunable spectra and enhanced local field can be used for sensing, which is much more suitable for the modern nanobiotechnology architectures [9–20]. However, localised surface plasmon resonance (LSPR) sensors are with orders of magnitude lower sensitivity compared with propagating SPR sensors [8, 13]. Only when measuring refractive index change in the nanometer vicinity to the metal surface, the sensitivity of LSPR and SPR sensors can be approximately equivalent because the LSPR sensor has a much smaller sensing volume due to its 40–50 times shorter electromagnetic-decay length than that of the SPR sensors [21].

A fundamental limitation to all kind of surface plasmon sensors is the strong radiative and non-radiative dampings, which natively accompanies and weakens the plasmon resonance [3, 8, 22–24]. As a consequence of the strong dampings, plasmon resonances in the visible and near infrared region have a linewidth of typically tens to hundreds of nanometres, which results in a very low quality factor and limits the sensing performance fundamen-

Xing-Yuan Wang, Yi-Lun Wang, Suo Wang: State Key Lab for Mesoscopic Physics and School of Physics, Peking University, Beijing 100871, China
These authors contributed equally to this work.
Bo Li, Xiao-Wei Zhang: State Key Lab for Mesoscopic Physics and School of Physics, Peking University, Beijing 100871, China
***Corresponding Authors: Lun Dai, Ren-Min Ma:** State Key Lab for Mesoscopic Physics and School of Physics, Peking University, Beijing 100871, China
and Collaborative Innovation Center of Quantum Matter, Beijing, China, E-mail: renminma@pku.edu.cn, lundai@pku.edu.cn

tally [3, 25, 26]. The recently developed plasmon lasers showed that these dampings can be fully compensated by gain medium at the lasing state [27–38]. This intrinsic merit has great potential to enhance the performance of devices based on plasmonic resonance phenomena [39–45]. One example is the plasmon laser for gas phase detection where the mechanism of the sensing process relies on surface defect state modification of semiconductor material [46]. However, to our knowledge, the gain effect in surface plasmon refractive index sensing has not been studied so far. Surface plasmon refractive index sensor is the most extensively utilised optical biosensors, which requires the device operated stably in solution and in a preferred wavelength window of ~700–900 nm where the background absorption and scattering from biological mixtures and of water are minimal [10, 47].

Here we demonstrated, for the first time, a lasing-enhanced surface plasmon resonance (LESPR) refractive index sensor. The device with a record low plasmon lasing threshold of ~50 KW cm^{-2} was stably operated in solution at room temperature. Due to the coherence nature of the lasing surface plasmon, the emission quality factor is about 2300 at the emission wavelength of 700 nm providing very high intensity sensitivity to refractive index change. The figure of merit (FOM) of intensity sensing is 84,000, which is about 400 times higher than state-of-the-art surface plasmon resonance (SPR) sensor. We found that the high FOM originates from three unique features of LESPR sensors: high quality factor, nearly zero background emission and the Gaussian-shaped lasing spectra. Moreover, the propagating surface plasmons utilised in LESPR sensors are directly excited and localised in a wavelength scale footprint, which avoids the sophisticated setup required for the indirect generation of surface plasmons by phase match and fits the device in the modern nanobiotechnology architectures. The LESPR sensors may form the basis for a novel class of plasmonic sensors with unprecedented performance for a broad range of applications.

Figure 1a shows the schematic of the device and the measurement scheme. Comparing to the SPR sensors, an additional semiconductor layer is added between planar metal surface and analyte as the gain material. Under optical pumping, the excited carriers in the semiconductor recombine and radiate dominantly to surface plasmons due to Purcell factor (see Supplementary Fig. 1) [31, 46]. This excitation-relaxation generation process of surface plasmons avoids the sophisticated setup required for the indirect generation of surface plasmons by phase match. Furthermore, these directly generated surface plasmons are localised in a wavelength scale square shaped cavity whose feedback mechanism relies on the total internal reflection of surface plasmons at the nanosquare boundaries [31, 46, 48, 49]. The refractive index change of the analyte modifies the cavity resonance wavelength and thus the lasing wavelength. Due to the coherence nature of the lasing emission by amplification of the stimulated emission, the signal from such a LESPR sensor has a much narrower linewidth comparing to the SPR sensor. For a given resonance peak shift, there will be a dramatic intensity change at a certain wavelength (Fig. 1b).

Fig. 1c shows a SEM imaging of the fabricated device consisting of a CdSe nanosquare on top of an Au substrate separated by a few nanometers of MgF_2 (see 'Method' section). We chose CdSe as gain material for its near-infrared emission located in the biosensing preferred region of 700–900 nm [10, 47]. The Au is chosen because that it is much stable compared to silver. Although silver has a lower Drude damping rate and thus has been widely used in reported plasmon lasers [28–35], the greater reactivity of silver as compared to gold makes it less suitable for use in biologically relevant media as silver can be easily oxidised, altering the plasmonic behaviour of the device [10]. The CdSe nanosquares are synthesised via chemical vapour deposition method. High-resolution transmission electron microscopy (HRTEM) shows that the CdSe squares have a single-crystal wurtzite structure (Fig. 1d). The gold substrate is deposited by E-beam evaporation. HRTEM shows that the gold film is with polycrystalline face-centred cubic structure (Fig. 1e) where the grain size diameter is about 50 nm (see Supplementary Fig. 2). The selected area electron diffraction patterns of CdSe and gold substrate are shown Supplementary Fig. 3, which further confirm their high crystal quality. The high quality of the CdSe and Au is essential for our device operating at room temperature and with a low threshold.

Fig. 2a shows the 3D full wave simulation results of the gain effect in a LESPR sensor device. The pumping produces an increase in gain, which is simulated by increasing the imaginary part of refractive index of gain materials (See Method). The electric-field-intensity distribution of the calculated mode is shown in Supplementary Fig. 4. At a gain coefficient of zero, the cavity quality factor is about 20, which is mainly limited by the non-radiative Drude damping. With the increasing of the gain coefficient, the cavity quality factor increases by orders of magnitude, indicating that the Drude damping has been compensated by gain. Such a high cavity quality factor is desired for refractive index sensing. To map the scaling law of the lasing emission quality factor, we have measured over 60 devices with their physical volume spanning over two orders of magnitude (Fig. 2b). Due to the strong field confinement

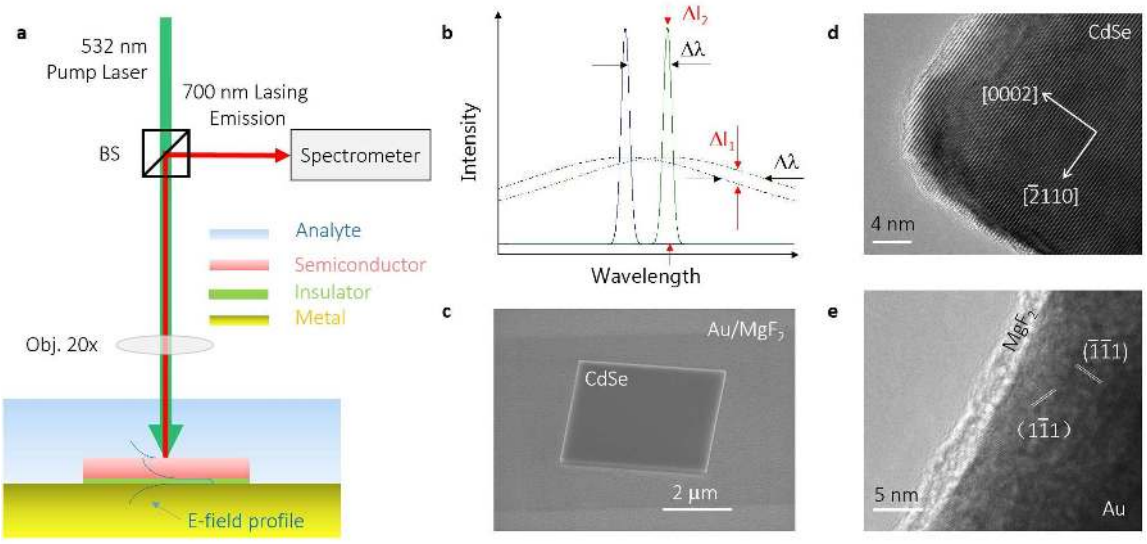

Figure 1: Measurement scheme, SEM and TEM of a lasing enhanced surface pleamon sensor (**a**) The schematic of the device and the measurement scheme. Comparing to the SPR sensors, an additional semiconductor layer is added between flat metal surface and analyte as gain material. Under optical pumping, the excited carriers in the semiconductor recombine and radiate dominantly to surface plasmons due to Purcell factor which avoids the sophisticated setup required for the indirect generation of surface plasmons by phase match. (**b**) A schematic showing that, for a given resonance peak shift, a resonance with narrower linewidth will have larger intensity change. Due to the coherence natural of the lasing emission by amplification of the stimulated emission, the signal from such a LESPR sensor has a much narrow linewidth comparing to the SPR sensor. For a given resonance peak shift, there will be a dramatic intensity change at a certain wavelength. (**c**) A SEM image of the fabricated device consisting of a CdSe nanosquare atop of Au substrate separated by a few nanometer MgF_2. The band edge emission of CdSe is around 700 nm locating in the biosensing preferred region. The Au is chosen because it is much stable comparing to silver. The scale bar is 2 μm. (**d-e**) High resolution TEM images for of CdSe nanosquare (**d**) and Au/MgF_2 substrates.

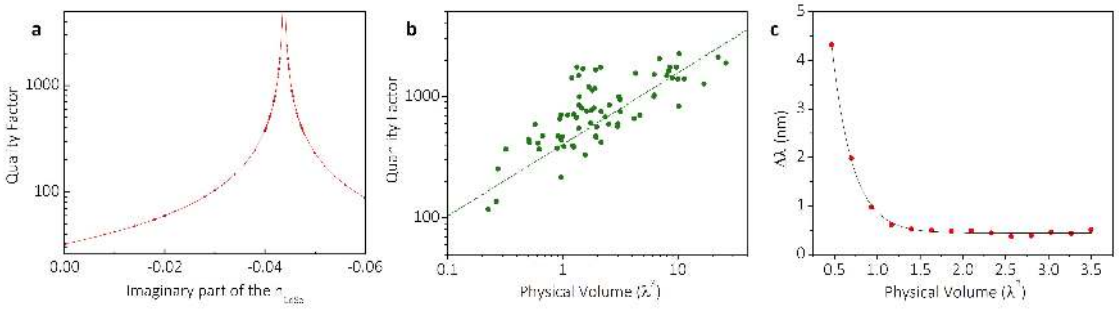

Figure 2: Loss compensation in a LESPR sensor by gain and analytes introduced resonant wavelength shift. (**a**) Full wave simulation result of the plasmon laser for the refractive index sensing. The pumping produced gain increasing process is mimicked by increasing the imaginary part of refractive index of gain materials. At a gain coefficient of zero, the cavity quality factor is about 20, which is mainly limited by the non-radiative Drude damping. With the increasing of the gain coefficiency, the cavity quality factor increases by orders of magnitude, indicating that the Drude damping has been compensated by gain. (**b**) Scaling law of the lasing emission quality factor. Over 60 devices with their physical volume spanning over two orders of magnitude were measured experimentally to map the lasing quality factor of LESPR device. (**c**) Full wave simulated wavelength shift of LESPR at a change of analyte refractive index of 0.0213. In our sensing scheme, the change of the environment refractive index produces a cavity resonance wavelength shift which can be monitored in the optical far-field in terms of lasing emission spectra. Such a shift becomes dramatic when the physical volume is smaller than λ^3.

of plasmonic effect, the quality factor is over 1000 at a volume of 10 λ^3, and can be over 100 at a deep subwavelength volume of 0.2 λ^3, where λ is the lasing wavelength of 700 nm. This quality factor scaling law not only guided us to design high-performance LESPR sensors, but also may help to design plasmonic nanolasers for other applications as well as understand ultrafast laser dynamics in a deep subwavelength cavity [50].

In our sensing scheme, the change of the environment refractive index produces a cavity resonance wavelength

shift, which can be monitored in the optical far-field as a shift either in the peak wavelength or in the intensity at a certain wavelength. Such a shift is related to the physical volume of the gain materials at a certain change of the refractive index. When the physical volume becomes smaller, there will be more electromagnetic fields located in the interaction medium, which will result in a large shift. As shown in Fig. 2c, such a shift becomes dramatic when the physical volume is smaller than λ^3.

The characterisation of LESPR sensors was performed in a chamber with two ports for exchange of solution with varying refractive indices and an optical window for both pumping and signal collection (See Method). The device has physical dimensions of 4 μm × 3 μm × 100 nm. All experiments were conducted at room temperature. Ethanol and propyl alcohol with refractive indices of 1.3588 and 1.3801 at 700 nm respectively are used to characterise the device. In both solutions, the device show typical lasing behaviour, while there is a clear lasing peak shift with altered refractive index (Fig. 3). The transitions from spontaneous emission to stimulated emission are verified from the non-linear response of the output power and gain saturation effect (Fig. 3c), linewidth narrowing effect (Fig. 3d) and lifetime evolution (see Supplementary Fig. 1) to the peak pump intensity. The threshold is about 50 kW cm^{-2}. As far as we know, this is the lowest threshold reported so far for plasmon lasers operated at room temperature [51–53]. Such a low threshold ensures the stable operation of the plasmon lasers in solutions as sensors.

Figure 4a shows the peak wavelength shifts of the lasing spectra with the refractive index after the onset of the lasing. While there is a slight blue shift of the lasing wavelength over the entire pump region owing to the free carrier plasma effect (see Supplementary Discussion 1), the absolute value of the wavelength shift is independent of the pumping power, indicating the stable performance of the devices. We note that the spontaneous emission wavelength is inert to environmental refractive index compared to stimulated emission, and can be seen as a background noise for sensing. However, due to the intrinsic nonlinearity in lasing process, the lasing peak has orders of magnitude higher intensity and narrower linewidth and thus can be easily separated from spontaneous emission by multi-peak data-fitting process (see Supplementary Fig. 5). The spectra at full lasing state with spontaneous emission subtracted in ethanol and propyl alcohol are plotted in Fig. 4b, which shows a pronounced red shift with the increase of the refractive index of the solution. We note that the spectra are asymmetrical due to the surface imperfection scattering induced coupling between clock-wise and a counter-clock-wise mode. And thus dual Gaussian peak fitting is used to fit these asymmetry spectra. The lasing linewidths in both solutions are about 0.3 nm, which corresponds to a quality factor of about 2300.

Two key parameters, sensitivity and figure of merit, are employed to characterise the performance of the lasers at full lasing state. The sensitivity of a sensor is defined as the rate of change of the information parameter (wavelength λ, or intensity I, here) magnitude measured with the analyte refractive index n. Depending on the regarded spectral region and the detection method, the sensitivity of an information parameter is not a sufficient measure because the absolute value of the information parameter magnitude measured is also a crucial factor for a sensor. An important comparative dimensionless quantity defined as the figure of merit FOM_P is further used, which takes into account the sharpness of the resonance and thus examines the ability to sensitively measure tiny information parameter changes. For the wavelength sensing, the sensitivity S_λ and FOM_λ can be calculated according to $S_\lambda = \Delta\lambda/\Delta n$ and $FOM_S = \left|\frac{\Delta\lambda/\Delta n}{FWHM}\right|$ respectively, where FWHM is the full width at half maximum of a lasing peak. For the intensity sensing, the sensitivity S_I and FOM_I can be calculated according to $S_I = \Delta I(\lambda)/\Delta n(\lambda)$ and $FOM_I = max\left|\frac{\Delta I(\lambda)/\Delta n(\lambda)}{I(\lambda)}\right|$, respectively [25, 54]. For the LESPR sensor, the wavelength sensitivity is obtained to be about 21 nm/RIU. While this sensitivity is moderate compared to LSPR and SPR, the narrow lasing linewidth produces a FOM_λ of LESPR about 70, which is high than the theoretical calculated FOM_λ for LSPR sensors (~20) and of state-of-the-art SPR sensors (~50) (see Supplementary Discussion 2) [3, 25].

For the intensity sensitivity S_I and FOM_I, a narrow linewidth and low initial signal intensity are crucial. Thus, the narrow lasing emission linewidth and the separation of the lasing emission from the spontaneous emission is anticipated to give a superior performance to LESPR sensor. Remarkably, we found that the lasing emission profile is another key factor to enhance the performance significantly. As shown in Fig. 4b, the lasing emission has a Gaussian shape, which is in stark contrast with the Lorentz-shaped SPR and LSPR resonances. For the same FWHM, Gaussian profile confines much better to the peak centre compared to the Lorentzian profile. As a consequence, a certain shift of the lasing peak due to the refractive index change will result in a more significant intensity change at a fixed wavelength. Indeed, the LESPR sensor has a superior performance in intensity sensing. The intensity detection figure of merit of our device is ~84,000, which is more than 400 times higher than state-of-the-art SPR sensors at same wavelength (See Supplementary Discussion 3) [3, 8].

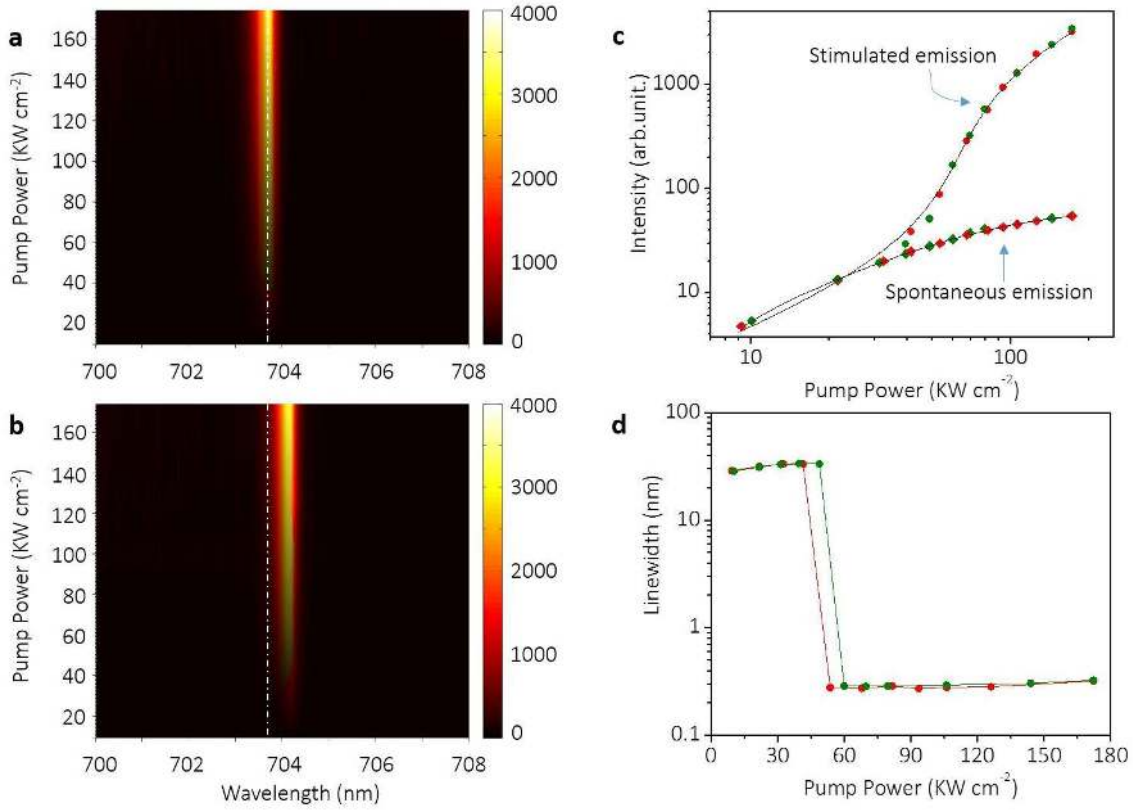

Figure 3: Optical far-field characterisation of LESPR sensor. (**a-b**) The emission spectrum evolution of a LESPR device in varied refractive index environment of ethanol (**a**) and propyl alcohol (**b**). At a fixed refractive index of interaction layer, the device show typical lasing behaviour, while there is a clear lasing peak shift with altered refractive index. (**c**) The light-light curves of the LESPR device shown in (**a-b**). The spontaneous emission becomes saturated after the onset of lasing due to the gain saturation effect, while the stimulated emission experiences a nonlinear increase to the fully lasing state. Data points in olive: device in ethanol; Data points in red: device in propyl alcohol. (**d**) The linewidth evolution with the pump power. There is a significant line width narrow width narrowing effect from a FWHM of ~20 nm below threshold to ~0.3 nm above. Olive: device in ethanol; Red: device in propyl alcohol.

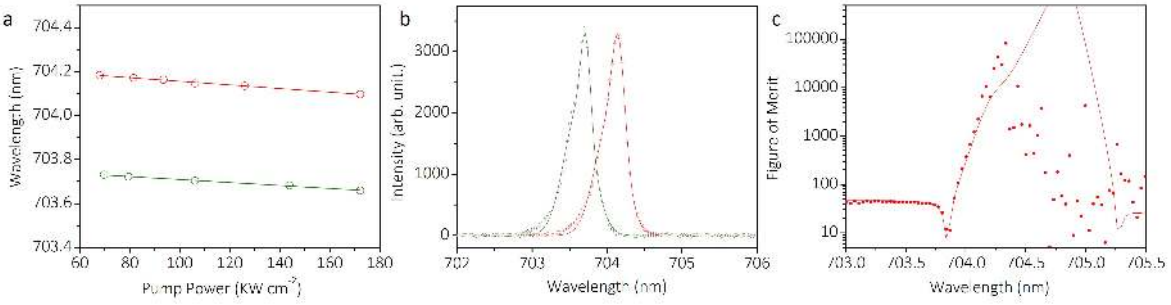

Figure 4: Sensitivity and figure of merit of a LESPR sensor. (a) The emission peak wavelength evolution of a LESPR device in varied refractive index environment. While there is a slight ~0.08 nm blue shift of the lasing wavelength over the entire pump region owing to the free carrier plasma effect, the absolute value of the wavelength shift about ~0.43 nm is independent of the pumping power, indicating the stable performance of the devices. Olive: device in ethanol; Red: device in propyl alcohol. (**b**) The spectrum shifts with the refractive index at fully lasing state. Olive: device in ethanol; Red: device in propyl alcohol. (**c**) The intensity detection figure of merit of LESPR device is ~84000, 400 times higher than state-of-the-art surface plasmon sensor at same wavelength. Such a record high FOM_I originates from the three exclusive features of LESPR sensor comparing to their SPR and LSPR sensors counterparts: extremely narrow linewidth, nearly zero background emission by decoupling of the lasing emission and spontaneous emission and the Gaussian shape of the lasing emission.

Further work, such as coating with appropriate functional molecules on the LESPR sensor, will be needed to explore the functionality of the sensor in various detection environment.

While both LESPR sensor and the recently reported plasmon laser gas sensor [46] show superior performance than their passive counterparts respectively, the detection mechanism of them are different. The mechanism of the plasmon laser gas sensor relies on surface defect state modification of semiconductor material. Consequently, its sensitivity is related to the electron deficiency of adsorbed molecules. LESPRs operate on the principle that changes in refractive index at the vicinity of the device surface results in a shift of the lasing spectrum.

In conclusion, we have experimentally demonstrated a novel class of sensors based on lasing surface plasmon resonance phenomena. We showed that the spectra linewidth of LESPR can be over two orders of magnitude narrower than those of the Drude damping limited SPR and LSPR. Together with the other two revealed features of LESPR sensor of the nearly zero background emission and Gaussian-shaped spectra, the LESPR showed an intensity detection figure of merit of 84,000, which is more than 400 times higher than state of the art SPR sensors. Furthermore, the propagating surface plasmons in LESPR sensors are directly excited and localised in a wavelength scale footprint, which avoids the sophisticated setup required for the indirect generation of surface plasmons by phase match and fits the device in the modern nanobiotechnology architectures. Our LESPR sensors may form the basis for a novel class of plasmonic sensors with unprecedented performance for investigating biomolecular interactions, biological and chemical sensing, national security, medical diagnostics, environmental monitoring and other applications.

Method

Numerical Mode Simulations:

The optical modes of the lasing enhanced surface plasmon sensors are calculated using a finite-element method 3D eigenmode solver (Comsol Multiphysics). In this model, the CdSe nano-square (n_{CdSe}= 2.8) lies in contact with a 5 nm MgF_2 (n_{MgF2}= 1.38) gap layer above an Au substrate (ε_{Au}= −16.486 – 1.0643i). The effective mode volume of the lasing plasmon cavity is calculated as: $V_{eff}=\frac{\int w_{em}(\vec{r})d^3\vec{r}}{\varepsilon_0\varepsilon(|\vec{E}|^2_{max})}$, where w_{em} is the electromagnetic energy density of the mode. $\vec{E}$ in the denominator is the evaluated maximal electric field. Taking into account the strongly dispersive property of silver, $w_{em}\left(\vec{r}\right)$ equals to $\frac{1}{2}[\mathrm{Re}\left[\frac{d(\omega\varepsilon)}{d\omega}\right]\left|\vec{E}\left(\vec{r}\right)\right|^2+\mu|\vec{H}(\vec{r})|^2]$. The Q factors of the cavity modes are calculated from the formula Q =$f_r/\Delta f$, where the f_r is the resonance frequency and Δf is the full width at half maximum of the resonance spectrum. For the Q factors of the cavity modes with introduced gain, a complex refractive index of n_{CdS}= n – iκ is set, where the gain coefficient κ can vary depending on the pump intensity. The Q factor is significantly enhanced by orders of magnitude with the increasing gain coefficient κ and reaches maximum at a κ value of about −0.0437.

Sample preparation.

The CdSe nanosquares were synthesised using a chemical vapour deposition method. CdSe (99.995%) powders were used as the source, and pieces of Si wafers covered with 5-nm-thick thermally evaporated Au catalysts were used as the substrates. The as-grown CdSe nanosquares had a single-crystalline lattice structure with a wurzite crystal lattice (Fig. 1b). The Au/MgF2 substrates for the fabrication of LESPR devices were deposited by electron-beam evaporation. The thickness of MgF_2 and Au film is 5 nm and 200 nm, respectively. HRTEM shows that the gold film is polycrystal where the grain size is about 50 nm (SOM). CdSe nanosquares were first deposited in solution and then spin coated onto the Au/MgF_2 substrates.

Device Measurement:

The characterisation of LESPR sensors was performed in a chamber with two ports for exchange of solution with various refractive indices and an optical window for both pumping and signal collection. Ethanol and propyl alcohol with refractive indices of 1.3588 and 1.3801 at 700 nm respectively are used to characterise the device. The devices are optically pumped by a nanosecond laser with λ_{pump} =532 nm, a 1 kHz repetition rate and approximately 4.5 ns pulse length. A 20× objective lens (NA=0.4) is used to focus the pump beam to a ~10 μm diameter spot onto the sample and collect the luminescence. The device characterised in Fig. 3 and 4 is with a physical dimensions of 4 μm × 3 μm × 100 nm. All experiments were conducted at room temperature.

Acknowledgement: This work was supported by the 'Youth 1000 Talent Plan' Fund, National Basic Research Program of China (No. 2013CB921901, and 2012CB932703), Ministry of Education of China (No. 201421) and the Na-

tional Natural Science Foundation of China (Nos. 11574012, 61521004, 61125402, 51172004, and 11474007).

References

[1] Maier, S. A. Plasmonics: Fundamentals and Applications (Springer, 2007).
[2] Liedberg, B., Nylander, C. & Lundstrum, I. *Sensors Actuators B* **4**, 299-304 (1983).
[3] Homola, J. *Surface Plasmon Resonance Based Sensors* (Springer, 2006).
[4] Anker, J. N. *et al. Nature Mater.* **7**, 442-453 (2008).
[5] Stewart, M. E. *et al. Chem. Rev.* **108**, 494-521 (2008).
[6] Stockman, M. I. *Science* **348**, 287-288 (2015).
[7] Prasad, P. N. *Introduction to Biophotonics* (John Wiley & Sons, 2003)
[8] Shalabney, A. & Abdulhalim, I. *Laser Photonics Rev.* **5**, 571–606 (2011)
[9] Yanik, A. A., *et al. Nano Lett.* **10**, 4962–4969 (2010).
[10] Nusz, G. J., Curry, A. C., Marinakos, S. M., Wax, A. & Chilkoti, A. *ACS Nano* **3**, 795–806 (2009).
[11] Peng, G., *et al. Nature Nanotechnology* **4,** 669-673 (2009).
[12] Liu, N., Tang, M. L., Hentschel, M., Giessen, H., Alivisatos, A. P. *Nature Materials* **10** 631-636 (2011).
[13] Kabashin, A. V., *et al.Nature Materials* **8**, 867-871 (2009).
[14] Cubukcu, E.; Zhang, S.; Park, Y.-S.; Bartal, G.; Zhang, X. *Applied Physics Letters* **95**, 043113 (2009).
[15] Li, J. F., *et al. Nature* **464**, 392-395 (2010).
[16] Mayer, K. M., Hafner, J. H., *Chem. Rev.* **111**, 3828–3857 (2011).
[17] Yanika, A. A., *et al. Proc. Natl. Acad. Sci.* **108**, 11784-11789 (2011).
[18] Brolo, A. G., *Nature Photonics* **6**, 709-713 (2012).
[19] Li, N., *et al. Light: Science & Applications* **3**, e226 (2014).
[20] Dantham, V. R., *et al. Nano Lett.* **13**, 3347–3351 (2013).
[21] Haes, A. J., Van Duyne, R. P. *Anal. Bioanal. Chem.* **379**, 920–930 (2004).
[22] Liu, N., *et al. Nature Materials* **8**, 758-762 (2009).
[23] Lassiter, J. B., *et al. Nano Letters* **10**, 3184–3189 (2010).
[24] Stockman, M. I., *Opt. Express* **19**, 22029-22106 (2011).
[25] Becker, J., Trugler, A., Jakab, A., Hohenester, U., Sonnichsen, C. *Plasmonics* **5**, 161–167 (2010).
[26] Novo, C. *et al. Phys. Chem. Chem. Phys.*, **8**, 3540–3546 (2006).
[27] Bergman, D. J. & Stockman, M. I. *Physical Review Letters* **90**, 027402 (2003)
[28] Hill, M. T. *et al. Optics Express* **17**, 11107-11112 (2009).
[29] Noginov, M. A. *et al. Nature* **460**, 1110-1113 (2009).
[30] Oulton, R. F. *et al. Nature*, **461**, 629-632 (2009).
[31] Ma, R.-M.; Oulton, R. F.; Sorger, V. J.; Bartal, G.; Zhang, X. *Nature Materials* **10,** 110-113 (2011).
[32] Khajavikhan, M. *et al. Nature* **482**, 204–207 (2012).
[33] Lu, Y.-J. *et al.Science* **337,** 450-453 (2012)
[34] Ma, R.-M.; Yin, X. B., Oulton, R. F.; Sorger, V. J.; Zhang, X. *Nano Letters* **12,** 5396-5402 (2012).
[35] Zhang C, Lu YH, Ni Y, *et al. Nano Letters* **15**, 1382-1387 (2015).
[36] Lakhani AM, Kim M-k, Lau EK, *et al. Optics Express* **19**, 18237-18245 (2011).
[37] Wei, Z., *et al*. *Nature Nanotechnology*, **8**, 506-511 (2013).
[38] van Beijnum, F., *et al*. *Physical Review Letters*, **110**, 206802 (2013).
[39] Lawandy, N. M. *Applied Physics Letters* **85**, 5040 (2004).
[40] Gordon, J. A. & Ziolkowski, R. W. *Optics Express* **15**, 12562-12582 (2007).
[41] Li, Z.-Y. & Xia, Y. *Nano Letters* **10**, 243-249 (2010).
[42] Hess, O., Pendry, J. B., Maier, S. A., Oulton, R. F., Hamm J. M. and Tsakmakidis, K. L. *Nature Materials* **11**, 573-584 (2012).
[43] Tame, M. S., McEnery, K. R., Özdemir, S. K., Lee, J., Maier, S. A. and Kim, M. S. *Nature Physics* **9** 329-340 (2013).
[44] Hess, O. and Tsakmakidis, K. L., *Science* **339** 654-655 (2013).
[45] Ye, D., Chang, K., Ran, L. & Xin, H. *Nature Communications* **5:5841** doi: 10.1038/ncomms6841 (2014).
[46] Ma, R.-M., *et al. Nature Nanotechnology* **9**, 600-604 (2014).
[47] Weissleder, R. *Nat. Biotechnol.* **19**, 316–317 (2001).
[48] Guo, W. H, Huang, Y. Z., Luo, Q.Y. & Yu, L.J. *IEEE Journal of Quantum Electronics*, **39**, 1563-1566 (2003).
[49] Huang, Y.-Z. *et al.*, *Optics letters* **33**, 2170-2172 (2008).
[50] Sidiropoulos TPH, Roeder R, Geburt S, *et al. Nature Physics* **10**, 870-876 (2014).
[51] De Leon, I. & Berini, P. *Nature Photon.* **4**, 382–387 (2010).
[52] Ma, R.-M., Oulton, R. F., Sorger, V. J. & Zhang, X. *Laser Photon. Rev.* **7**, 1–21 (2013).
[53] Hill, M. T., & Gather, M. C. *Nature Photonics* **8**, 908-918 (2014)
[54] Liu, N. Mesch, M., Weiss, T., Hentschel, M., Giessen, H., *Nano Letters* **10**, 2342-2348 (2010).